Environmental Science Nano

Improved Methodology for the Analysis of Polydisperse Engineered and Natural Colloids by Single Particle Inductively Coupled Plasma Spectroscopy (spICP-MS)

Journal:	*Environmental Science: Nano*
Manuscript ID	EN-ART-06-2023-000425.R1
Article Type:	Paper

SCHOLARONE™
Manuscripts

Environmental Significance

Broad size distributions are the norm for environmental nanoparticles and colloids. Although determining particle number concentration (PNC) and particle size distribution (PSD) is recognized as an important component of investigating the cycling and potential environmental impacts of nanoparticles and colloids, making these measurements is challenging for materials that can span the nanometer to micron size range in each sample. Particle counting techniques, notably single particle ICP-MS, must address the issue of extreme polydispersity to avoid possible artifacts. We examined how PSD and PNC can be successfully measured through the use of serial dilutions and data processing. We present two case studies to show the value of the technique for accurate measurements of PSD and PNC when studying nanoplastic behavior and interpreting hydrologic influences on aquatic colloids.

IMPROVED METHODOLOGY FOR THE ANALYSIS OF POLYDISPERSE ENGINEERED AND NATURAL COLLOIDS BY SINGLE PARTICLE INDUCTIVELY COUPLED PLASMA SPECTROSCOPY (spICP-MS)

Shaun Bevers[1], Casey Smith[2], Stephanie Brown[2], Nathan Malone[2], D. Howard Fairbrother[2], Aaron Goodman[1], and James F. Ranville[1].

[1]Department of Chemistry, Colorado School of Mines, Golden, CO 80401, United States

[2]Department of Chemistry, Johns Hopkins University, Baltimore, MD 21218, United States

Abstract.

Although nanomaterials (NMs), both natural (clays, mineral dust aerosols, etc.) and anthropogenic (nanoplastics, tire wear particles, etc.) have been recognized as a key component of environmental processes, their characterization and quantification in environmental matrices remains difficult. In contrast to monodisperse NM standards, environmentally-sampled NMs can contain a broad, continuous, polydisperse particle size distribution which creates analytical difficulties for many single particle counting techniques, including single particle inductively coupled plasma mass spectrometry (spICP-MS). By employing environmentally relevant, nanoplastics tagged with metals, as well as Al-bearing stream mineral colloids, we demonstrate the deleterious effects of particle-based backgrounds caused by coincident small particles on spICP-MS analysis of particle number concentration (PNC) and particle size distribution (PSD). A novel methodology is presented that successfully minimizes the effects of particle coincidence using serial dilutions to identify distortion-free segments of the PSD, which are combined and modeled using a power law distribution. The physical relevance of the parameters derived from power law modeling are demonstrated using suspensions of two different nanoplastics tagged with metals. Finally, this new methodology is applied to analysis of Al-bearing colloids sampled during a storm event in order to highlight the possible distortions present in a single dilution analysis. This comparison demonstrates the value of our proposed methodology for environmental NM and colloid analysis.

Introduction

Nanomaterials (NMs) are operationally defined by their size (1-100nm in one dimension), and display unique sized-based properties that collectively govern the reactions in which they participate and to what degree(1). The enhanced reactivity of NMs, as compared to their macroscopic counterparts, has led to the rapidly expanding field of nanotechnology, although some NMs (e.g. gold) have been used for millennia(2). Nanomedicine utilizes NMs with defined size and surface functionality to target specific cells/tissues for imaging(3) or drug-delivery(4). Nanoencapsulation of nutrients and pesticides to control release rates increases crop productivity compared to application of their dissolved counterparts, creating the burgeoning field of nano-agriculture(5). Natural NMs and incidental NMs (generated as a byproduct of human activity) are ubiquitous in the natural world(6). The size-based reactivity of NMs makes them potent substrates in a wide variety of environmental processes despite their low mass concentrations relative to their macroscale and dissolved counterparts(6).

The size-dependent reactivity of engineered, incidental and natural NMs can lead to undesired environmental consequences. The oxidation state and speciation of both inorganic and organic dissolved species can be tied to the high specific surface area of NMs, which is a function of size(7,8). Smaller, more mobile NMs can facilitate the environmental transport of both organic and inorganic contaminants(8–10), and micronutrients(11). Nanoplastics (NPs: 1-1000nm), generated from weathering of microplastics (< 5 mm), are a distinct and newly recognized class of incidental NM(12) that have greater environmental mobility and higher bioavailability than microplastics(13). Additionally, as a consequence of their high specific surface area, colloidal particles up to several microns are also a key component of environmental particle populations. Thus, to fully understand particle-mediated environmental processes, it is critical that accurate particle analysis and quantification be able to span orders of magnitude (nm – μm).

Particle toxicology(14) is intimately tied to size, which is the principal determinant of particle ingestion(15) and cellular uptake(4). Ultrafine aerosol particles (PM 0.1) are more toxic and persistent in human cells than their coarser counterparts (PM 2.5)(16,17). As a consequence of how reactive surface area scales with size, mass-based regulatory standards (mass/volume) for chemical exposures, which are generally applied for the preservation of aquatic life and aerosol particle exposure(18), are inadequate when describing the dosage of NMs. Rather, particle number or surface area may be better descriptors of dose. Indeed, measurements of mass concentration can equate to vastly different particle number concentrations (PNC) depending on their size and polydispersity(17). For these reasons, accurate measurement of PNC and particle size distribution (PSD) is essential to fully understand the ecological hazards and human health risks of NM exposure.

For monodisperse NMs, which often have Gaussian size distributions of particle numbers, determination of PSD and PNC is relatively trivial using techniques such as dynamic light scattering(19), analytical ultracentrifugation(20), field flow fractionation(21), or single-particle techniques such as nanoparticle tracking analysis (NTA)(22) and single particle optical sizing (SPOS)(23). However, both natural and incidental NMs, as well as colloids, are generated through a wide variety of physicochemical reactions that typically produce broad, continuous PSDs that range over orders of magnitude(6). Environmental particles have been shown to demonstrate size-dependent particle number distributions that often follow Pareto's Law (power law)(24–26):

$$\frac{\Delta N}{\Delta D_p} = \alpha\left(\frac{D_p}{\Delta D_p}\right)^{-\beta} \qquad \text{Eq 1}$$

where $\Delta N/\Delta D_p$ is the change in particle number with size, α and β are constants, and $D_p/\Delta D_p$ is particle diameter divided by the width of the size bin (ΔD_p). The constant α is a reflection of the magnitude of particle concentration and β describes the proportion of small to large particles (i.e. the PSD), and has been found to vary and reflect the mechanical, chemical and biological processes responsible for particle formation(26,27). Many of the aforementioned techniques are suitable for monodisperse particles but struggle to accurately size and/or count particles present in these continuous, polydisperse size distributions. Consequently, there is a need to develop new robust analytical approaches capable of accurately determining PSDs and PNCs for environmentally relevant NMs and polydisperse NPs.

Single particle inductively coupled plasma mass spectroscopy (spICP-MS) has seen increasing usage as a tool to characterize the PSD and PNC of metal-containing NMs and colloids(28–31). This technique takes advantage of the high elemental sensitivity and specificity of ICP-MS combined with a spray chamber

that allows for the introduction of intact, individual particles into the plasma. Instrument response is near-continuously monitored, with 100µsec dwell times (i.e., integration time) commonly being employed. Particles are ionized, and the resulting ion clouds register as discrete bursts of signal on the MS detector, which when resolved from the constant background signal, enable the counting and sizing of individual, submicron particles. However, discrimination between background and particle signals is not simple and involves setting a threshold value, with signals above this value being counted and sized as particles. Threshold values are generally set as the mean (µ) plus a multiple of the standard deviation (σ) for all measured signals. A threshold of $\mu + 3\sigma$ is widely used(28) and implemented in commercial analysis software, but other methods involving a variation of $\mu + x\sigma$(32,33) or modeling of background signal as a Poisson distribution have also been suggested(34,35).

The smallest detectable mass of the element of interest is fundamentally determined by instrument sensitivity and the threshold. Conversion of this minimum mass to particle size requires assumptions about the mass fraction of the element in the individual particle, the particle density, and its shape(36). High background signal, arising from dissolved elemental species, isobaric/polyatomic interference, or instrumental noise, increases the particle detection threshold, raising the lower limit of detectable particle size(37).

The upper limit of measurable particle mass fundamentally depends on two factors, ablation efficiency (AE), the ability of the plasma to completely ionize the particle, and transport efficiency (TE), the ability of the spray chamber to successfully aerosolize and transport the particle into the plasma. Both parameters decrease as a function of increasing particle size and density, leading to approximate upper limits of about 500nm for dense, recalcitrant silica particles(38) and 5um for low density microplastic particles(39).

Possible analytical artifacts in spICP-MS arise from particle coincidence and aggregation(34,40,41), both of which lead to overestimates of particle size and underestimates of PNC. Coincidence arises when two or more individual particles are introduced in the plasma within the same dwell times, whereas aggregation represents the physical association of multiple particles. Both are related to total particle concentration, and thus increasing dilution directly reduces the probability of coincidence while also making aggregation less favorable.

Despite the increasing number of applications of spICP-MS for NM characterization, polydisperse samples by their nature remain difficult to characterize by spICP-MS. Given a possible power law distribution of particle numbers by particle size, there can be exponentially more small particles for every large particle present. High concentrations of the very smallest particles can form a high background of coincident particles, with the consequence that the detection threshold is increased, effectively obscuring the smaller size range of the PSD. Addressing the challenge of accurate PNC and PSD measurement for polydisperse samples in the presence of a particle-based background is the central focus of this work. We propose an approach of analyzing polydisperse samples using spICP-MS, where PSDs from multiple dilutions are compared to determine particle size ranges that contain analyzable data in which artifacts due to coincidence are absent. As our results demonstrate, data from coincidence-free regions can be combined across a series of dilutions to model the entire, broad PSD using a power law. The results generated by power law modeling of the PSDs using this new serial dilution approach are contrasted with a commonly used, single dilution spICP-MS data analysis(42–46). To illustrate the benefits of this approach, we analyzed two types of environmentally relevant NMs:

polydisperse, metal-doped NPs which were used for method development; and Al-bearing NMs and colloids (i.e., silicate minerals) sampled during a storm event in the Denver Metro Area, CO USA.

Materials/Methods

Nanoplastic Synthesis. We have prepared a broad library of metal-tagged model NPs for use in experiments to probe the effect of size on environmental behavior of NPs (C. Smith et al., JHU manuscript in prep). We have utilized two NPs from this library to develop the spICP-MS methodology reported herein. Polydisperse, model NPs composed of polyvinylpyrrolidone (PVP) or polymethylmethacrylate (PMMA) containing ≈ 0.1 and 1% Ta by mass were manufactured for quantification by spICP-MS. To create these metal-doped NPs, a known mass of neat polymer and organometallic additive (e.g. $Ta(OC_2H_5)_5$) were dissolved in an organic co-solvent (Methanol and Toluene for PVP and PMMA, respectively) to create a solution which was cast in an aluminum dish. The organic solvent was then evaporated, leaving a metal-tagged composite. MicroXRF (Bruker M4), performed in the Minerals and Materials Characterization facility (MMC) at the Colorado School of Mines demonstrated that this approach leads to a uniform distribution of metal within the composite (C. Smith et al., manuscript in prep). This uniformity enables the metal signal in spICP-MS to be used to compute the size of NPs produced by cryo-milling the composites (details in SI). Aqueous suspensions of NPs were prepared through addition of dry powder to nano-pure water; the suspensions were sonicated and then sieved (<32 μm), producing stock solutions of polydisperse metal-tagged MPs.

Environmental NMs (Colloids). Cherry Creek, a tributary of the South Platte River, originates southeast of Denver near Castlewood Canyon, CO, and is impounded in Cherry Creek Reservoir. Daily grab sampling (5/19/22-5/23/22) of Cherry Creek surface water was performed to capture a major precipitation event (5/20/22-5/22/22). The sampling site in Denver CO was roughly equidistant from the confluence with the South Platte River and Cherry Creek Reservoir (39°41'43.7"N 104°55'14.3"W). Continuous discharge data (Q, cubic feet per second, SI Figure S1) was obtained from the USGS (Gauge: USGS 06713500 CHERRY CREEK AT DENVER, CO). Further details can be found in SI.

Nanoanalysis

Model NPs were imaged by scanning electron microscopy (TESCAN MIRA3 LMH Schottky field emission-scanning electron microscope (FE-SEM)) in the Minerals and Materials Characterization facility (MMC) at the Colorado School of Mines. Both model NPs and environmental NMs and colloids were analyzed by quadrupole spICP-MS (Perkin Elmer NexION 300D, Waltham, MA, USA) for ^{181}Ta or ^{27}Al content, respectively. Measurements employed 100 microsecond dwell times, a total measurement time of sizty seconds and size analysis utilized the mass-based approach to determine transport efficiency(28). TE was generally 5-8% throughout the study. Particle size was computed from the mass of ^{181}Ta or ^{27}Al detected in each particle, the mass percentage of this element in the particle, and the particle density. The low loading of Ta additive would not create an observable effect in the size calculation when using the polymer density, i.18 g cm^{-3} and 1.20 g cm^{-3} for PMMA and PVP respectively. Similarly XPS and FTIR showed no effect of the additive on the bonding within the polymer, also supporting the use of the polymer bulk density (smith et al , in prep). The ^{27}Al content of K-Feldspar, a common detrital mineral,

was used to estimate particle size for the river NMs and colloids. Additional details of data collection and analysis are provided in the SI.

Results and Discussion

Particle-Generated Background in Polydisperse Samples

As previously noted, accurately measuring sample PSD by spICP-MS revolves around finding a dilution that successfully minimizes particle coincidence. For monodisperse samples whose mean size is well above the threshold, the effects of particle coincidence on experimentally determined size and number can be easily identified across the measured PSD (see example in SI Figure S2). Using monodisperse standards as a basis, Abad-Álvaro et. al.(34) has suggested that nanoparticle and colloidal samples can be characterized at a single dilution that depends on the spICP-MS measurement conditions (nebulization efficiency, sample flow rate, dwell time, total acquisition time). For the conditions used in this study, this equates to ≈4000 particle events counted per analysis. Such an approach works well for relatively monodisperse (normally distributed) samples.

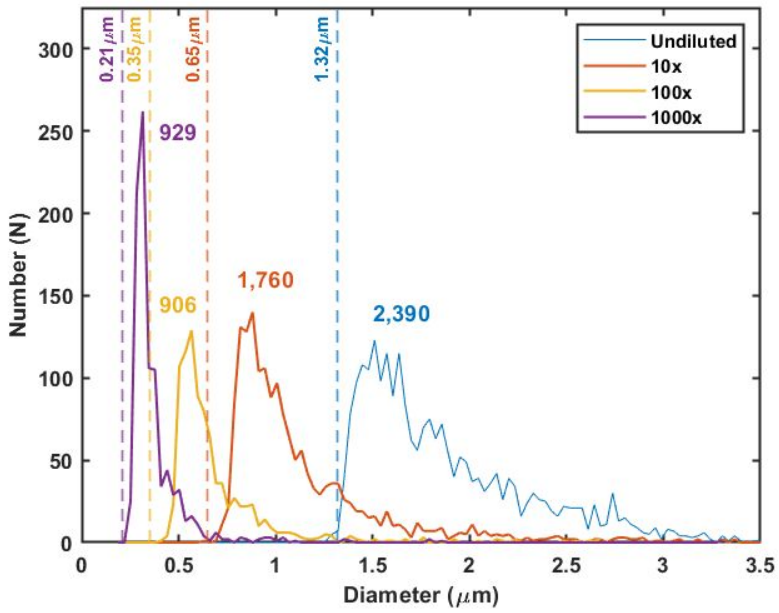

Figure 1. PSDs of 10-fold serial dilutions of a 0.1% Ta-Ethoxide Polyvinylpyrrolidone (PVP) suspension (Undiluted Nominal Concentration: 10.1mg/mL PVP). Threshold size (dashed line) and the particle no. detected (bold number) for each dilution is indicated. Detected particle number was not corrected for dilution. Particle diameters reflect a conversion of the measured mass of ^{181}Ta to an equivalent diameter of a PVP particle based on the (0.1 %) loading of Ta-Ethoxide and the polymer density (1.2 gm/cm^3).

Polydisperse samples such as our model NPs and natural stream particles, with particle numbers distributed over a broad continuum of sizes, pose a much greater challenge to accurate PSD/PNC measurement via a single dilution. For example, PSDs measured over serial 10x dilutions (ranging from undiluted to 10^3x) for a dispersion of 0.1% (w/w) Ta-Ethoxide doped PVP plastic NPs are shown in Figure 1. Clearly the reported PSD is influenced by dilution. The clearest indication of a coincidence-induced artifact is the change in the minimum observable size of the PSD. The threshold particle size (μ + 3σ) of the undiluted sample was 1.32μm. At the maximum dilution this is reduced to 0.21μm. This value was calculated based on the amount of Ta mass present in 1 count, the smallest denomination of signal measurable by the ICP-MS. The dissolved Ta calibration curve was used to calculate the amount of Ta mass represented by 1 count, which was converted into an equivalent mass of PVP (see Equation 1 in SI) given the 0.1% (w/w) content of Ta-Ethoxide present in the PVP plastic.

PNCs are affected by dilution as well, with increasing PNC as dilution is increased. In the undiluted and 10x dilutions, 2,390 and 1,760 particles were counted respectively, demonstrating that an additional 1,521 particles were measured over the 239 that were expected to result from the 10x dilution. Thus, total particle number did not decrease proportionally with a 10x dilution, and subsequent dilutions follow this same trend of showing "excess" particles at each step. Clearly not all of the particles are being counted in the more concentrated samples. In a well-behaved system bereft of coincidence, particle numbers should scale linearly with dilution and the PSD should remain constant. In the case of these polydisperse Ta-PVP NPs, the reason for the non-linear scaling in particle numbers can be attributed to experimentally determined threshold values being greater than the theoretical value of 0.21 um. This artifact is a result of coincident small particles that elevate the thresholds. As the dilution increases, the probability of coincidence decreases and the threshold drops. Consequently, smaller particles become observable, and are now counted as individual particles, causing the experimentally observed PNC to increase. Additional evidence of an elevated background arising from coincidence is the absence of a detectable ^{181}Ta signal following 0.02 µm filtration of the undiluted sample. This observation supports the conclusion that the thresholds greater than 0.21 µm are generated by coincident nanoparticles and not a consequence of ionic ^{181}Ta or small, undetectable NPs (< 0.02µm).

The observation of increasing particle numbers and changing observable particle size as a function of dilution-induced threshold reduction is characteristic of a particle-based background. In contrast, for a threshold derived from dissolved ions, it should be possible to find a dilution where the background is reduced to a point where pulses generated by the smallest particles can be resolved and quantified. For this Ta-doped PVP suspension, proportional dilution of total particle number never occurs, as shown by the nearly equal particle numbers (906 and 929) measured in the two highest dilutions: 10^2x and 10^3x respectively. This observation indicates that coincident particles smaller than the theoretical value of 0.21µm are present. Further dilution may achieve proportional dilution, but PNCs would be very low. Numerous studies have been dedicated to the resolution of particle signals from a background composed of dissolved ions, but few have discussed the presence of a background composed of coincident particles(47). Although each dilution (Figure 1) comfortably has <4000 events, a criterion that has been suggested in the past(34,48) as necessary for avoiding coincidence in mono-dispersed samples, our results suggest that this criterion may not extend to highly polydisperse samples.

Our results (Figure 1) highlight that while dilution can successfully lower the threshold, it concurrently reduces counting statistics for the largest particles, drastically limiting the upper range of observable particle size, particularly at the high dilutions needed to quantify the smallest particles. Finding a single, perfect dilution that maximizes measurement range while minimizing the particle coincidence may not be feasible in highly polydisperse samples. Techniques such as hydrodynamic chromatography (HDC)(49) or field flow fractionation (FFF)(50) have been used in combination with spICP-MS to provide physical separation by particle size. Feasibly, this would allow for the separation and quantification of any particle-based background, but in practice both techniques greatly dilute the injected sample, resulting in insufficient particles to count during spICP-MS.

Making Use of Imperfect Data: Partial, Proportional Sample Dilution and Power Law Modeling

As demonstrated by Figure 1, coincidence is a major concentration-induced cause of PSD distortion in spICP-MS that results in PNC undercounting and an erroneously larger PSD due to the summation of coincident particle masses. Furthermore, these distortions are more likely to occur in the lower region of

the PSD (Figure 1) as the smaller particles are found at much greater concentrations in polydisperse samples. Moreover, the effect on the measured particle mass is increased proportionately more when two small particles are coincident than when one or more small particles are coincident with a much larger particle.

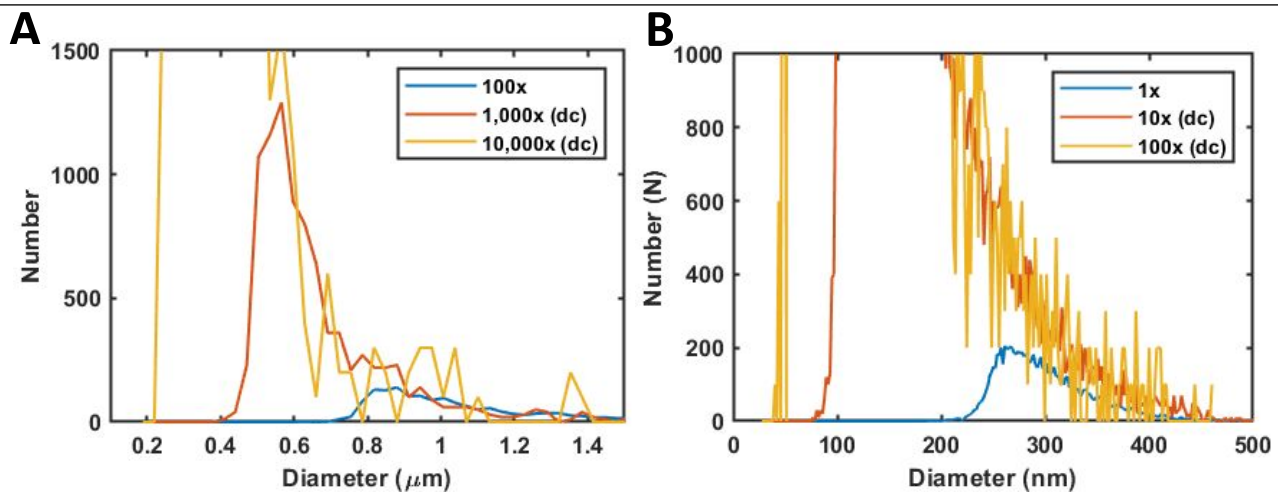

Figure 2. Dilutions of a 0.1% Ta-Ethoxide PVP suspension (nominal initial concentration of 8.8 mg/mL PVP) (Panel A) and an Al-containing environmental colloid (Panel B) sampled from Cherry Creek, Denver CO on May 20th 2022. Particle diameters reflect the equivalent size of PVP particles given the loading of Ta-Ethoxide (Panel A) or the equivalent size of K-Feldspar given the percent composition of Al (Panel B). For each dilution the particle numbers were normalized to lowest dilution (100x), denoted by (dc: dilution corrected).

Figure 2A shows the PSD of three different dilutions of a 0.1% Ta Ethoxide PVP suspension where the particle numbers of the two higher dilutions are normalized to the lowest (10^2 x) dilution factor. With each dilution, increasingly smaller particles are uncovered because the threshold decreases, showing that the functional form of the PSD is sensitive to the dilution. Examining the PSD of the three dilutions, it is apparent that there are, however, regions of disproportional and proportional dilution. For example, between particle diameters of 0.9-1.5µm, the dilution-corrected particle numbers of all three dilutions agree, demonstrating that in this size regime there is proportional dilution of particle number. In contrast, at particle diameters 0.75-0.9µm, the dilution corrected particle numbers of the 10^3x dilution do not agree with those of the 10^2x dilution, which is attributable to the combined effects of the coincidence in the smaller size range of the 10^2x dilution PSD and the higher threshold. Agreement is seen between the 10^3x and 10^4x dilutions above 0.5µm, but a lower detectable size limit of about 0.4µm in the 10^3x dilution is apparent.

The dilution-corrected PSD for an Al-bearing colloid sampled from Cherry Creek, Denver CO USA (Figure 2B) illustrates another facet of this type of analysis. Unlike the previous example, no portion of the dilution-corrected PSD of the 10^1x and 10^2x dilutions overlap with the undiluted sample, suggesting that the entire PSD measured for the undiluted sample is coincident. This conclusion is supported by similar effects seen in monodisperse samples at high concentrations where coincidence and aggregation distort the entire PSD (SI Figure S2). In contrast, over a range of particle sizes spanning 0.2-0.5µm, the dilution-corrected particle numbers of the 10^1x and 10^2x dilution of this Al-bearing colloid agree, suggesting the absence of concentration-dependent effects within this region. In other words, these overlapping

regions between different dilutions where the dilution-corrected particle size distributions are coincident can be considered "artifact-free" and undistorted either partially or wholly by coincidence and/or aggregation. The identification of these regions is the essence of our new approach and is the necessary step towards finding the "artifact-free" PSD and PNC for a polydisperse sample.

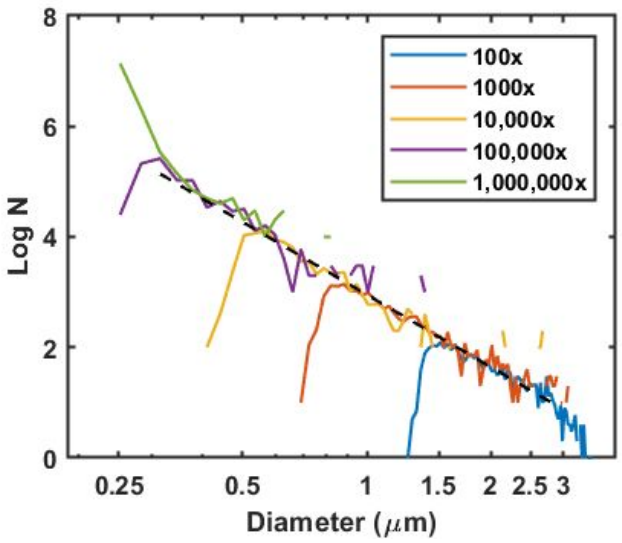

Figure 3. Log-log plot of PSD for 10-fold dilutions (10^2x – 10^6x) of a 0.1% Ta-Ethoxide PVP suspension using spICP-MS (nominal undiluted concentration: 8.8mg/mL). Higher dilutions were normalized to the original 10^2x dilution. The model (black dashed line) is the linear regression of the power law model of particle number vs particle diameter (see text for details).

Using this approach, we can use multiple dilutions to identify regions of the PSD in each dilution where particle numbers are proportionally diluted and thus are free of coincidence. As shown in Figures 1 and 2, this results in each dilution representing a different viewing window into the "artifact-free" PSD. Ideally these windows can be combined into a larger picture of the "artifact-free" PSD over all measured particle size ranges across all dilutions.

The power law model of particle number versus particle size (Equation 1) has been successfully used in the past to model polydisperse PSDs in natural samples(24,25). In this model, particle number is a function of particle diameter raised to a constant β, which itself is related to the distribution of particle numbers across the measured PSD (i.e. the proportion of small to large particles). The constant α is related to the total number of particles in the sample (i.e. PNC). Although power law models have been applied to data from other particle sizing techniques(25,51,52)it was only recently applied to modeling spICP-MS measurements of mineral dust aerosols(47). In the current case of the metal-tagged NPs, we use the power law to model polydisperse PSDs across a range of dilutions so that its shape and PNC can be compared independent of particle-generated thresholds at each dilution (Figure 1) and particle coincidence (Figure 2B).

The power law relationship (eq 1.) is linearized by log transformation, resulting in:

$$\log N = \log \alpha + \beta \log D \qquad \text{Eqn. 2}$$

A plot of spICP-MS data as the log of particle number, N, versus the log of particle diameter, D, will therefore have a slope of β and a y-intercept of log α. The value of α increases in response to increasing PNC. For these spICP-MS datasets, bin size was consistently 1nm so the term ΔD_p from Eqn. 1 can effectively be ignored.

Determining the "artifact-free" Size Distribution of metal-tagged NPs: We employed the power law analysis approach for spICP-MS data of metal tagged NPs. A log-log plot for a dilution series of 0.1% Ta-Ethoxide PVP suspended NPs (Figure 3) shows both rapid change in particle number near the threshold

as well as regions of proportional dilution, the latter being the regions of each dilution's PSD that is free of distortion (i.e., "artifact-free" PSD regions). The "artifact-free" PSD regions specifically identified for dilutions of 10^5x, 10^4x, 10^3x, and 10^2x were: 0.31-0.76µm, 0.76-1.13µm,1.13-1.57µm, and 1.57-2.8um, respectively. The PSDs from each of these dilutions were combined, creating a "artifact-free" PSD spanning particle diameters of 0.31 – 2.8µm. The lower limit of PSD used from the 10^5x dilution, 0.31µm, was derived from the overlap in dilution corrected PSD between the 10^5x dilution and a 10^6x dilution. No data from the 10^6x dilution was incorporated into the power law fit as there was no higher dilution with which to compare.

Given the fidelity of the linear relationship between particle number and size on the log-log plot for particle sizes ranging from 0.31 – 2.8µm across the dilution series (R^2 = 0.982), it suggests that the power law should continue beyond 2.8µm in particle diameter. However, this regime cannot be quantified by spICP-MS because decreasing particle transport efficiency into the spICP-MS results in undercounting at sizes >2.8µm. The specific particle size at which transport efficiency begins to affect the PSD measured by spICP-MS depends on the particle's physical properties such as density and surface hydrophobicity. Previously, a transport efficiency of 0.04% was reported for more hydrophobic 2.5µm-diameter PS beads using a cyclonic spray chamber(53) but in the present study the linear relationship between particle number and diameter continues from 2.5-2.8µm, suggesting somewhat efficient transport of hydrophilic PVP particles <2.8µm in diameter. It should be noted that ablation efficiency is not expected to affect the PSD measured in this experiment as previous studies have shown complete ablation of plastic microspheres up to 5µm in diameter(39), significantly larger than any of the particles analyzed in the present study.

Linear regression of the combined PSDs presented in Figure 3 resulted in values of 4.956 and -4.5638 for log α and β, respectively, and a power law model relating particle number to particle diameter of:

$$N = 10^{4.956} D^{-4.5638} \qquad \text{Eqn. 3}$$

Residuals of the linear regression of the log-log plot fit (SI Fig S3) show no systematic, size-dependent deviation, suggesting that a log-log plot of the combined dataset is well modeled by linear regression. The high $-\beta$ value reflects a broad size distribution with a high proportion of small to large NPs. Using equation 3 to replot the power law model over the original PSD data set for three dilutions shows good agreement (SI Figure S4). Given these results, we believe that the power law successfully models the relationship between particle number and particle diameter for this suspension of mechanically generated, metal-tagged PVP NPs.

β Values reflect Physical Characteristics of the Measured PSDs: A central question regarding the β value is whether it reflects a difference in physical properties between two sample populations, as measured through the shape of their PSDs. Both the PVP (1% (w/w) Ta-Ethoxide) and PMMA (0.1% (w/w) Ta-Ethoxide loading) model NPs were created through the same casting, cryo-milling, and sieving processes, but due to their different mechanical properties, the resulting NPs were expected to have different PSDs(54,55). The results of four dilutions of a 1% Ta-Ethoxide PVP suspension, and two dilutions of a 0.1% Ta-Ethoxide PMMA suspension are presented in Figure 4A and 4B, respectively.

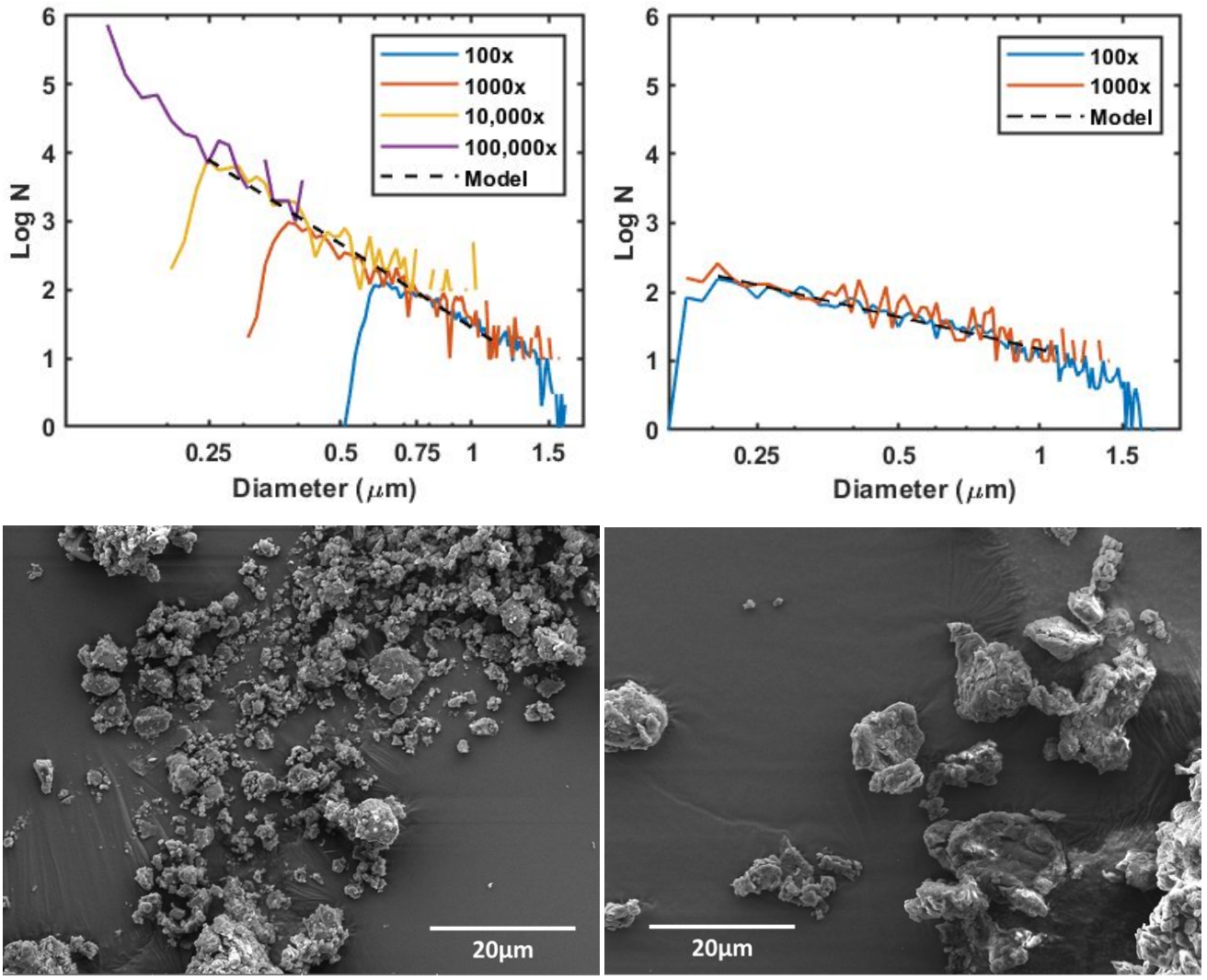

Figure 4. Log-log plots of (10^2-10^5x) dilutions of a 1% Ta-Ethoxide PVP (Panel A), and 10^2x and 10^3x dilutions of a 0.1% Ta-Ethoxide PMMA suspension (Panel B). For each dilution the particle numbers were normalized to lowest dilution. SEM micrographs of the dry 1% Ta-Ethoxide PVP (Panel C) and 0.1% Ta-Ethoxide PMMA powder (Panel D) mounted on carbon tape and sputter coated with Au.

Utilizing the overlapping PSD regions from three dilutions (10^2-10^4x) of the PVP suspension, linear regression of log N versus log D yielded values of -4.06 ± 0.09 and 3.45 ± 0.02 for β and log α, respectively (R^2 = 0.974). From the overlapping PSD regions of the two PMMA dilutions, values of -1.55 ± 0.06 and 2.17 ± 0.02 for β and Log α, respectively, were obtained (R^2 = 0.916). The more negative value of β for the PVP (-4.06) compared to the PMMA (-1.55) indicates that particle numbers increase more rapidly with decreasing size for the PVP suspension. This lower β (i.e. a lesser increase in the proportion of small to large particles) for the PMMA is consistent with near complete overlap between the dilution corrected 10^3x and 10^2x PSDs across the entire particle size regime. Further dilution of the PMMA was not possible due to low overall PNC in the undiluted suspension, although the overlap between the two dilutions suggested no further dilution was necessary. SEM micrographs qualitatively support the

inference from spICP-MS that the PVP sample shows proportionally larger numbers of smaller particles as compared to the PMMA sample. Thus, the average size of particles in the SEM micrographs is clearly larger for the PMMA compared to the PVP NPs. It should be noted that the SEM images depict particles larger than the upper measurement range of the spICP-MS, but the relative trend in particle number as a function of particle size can reasonably be expected to extend to larger particle sizes given the success of the power law in modelling the PSD for PVP and PMMA in the size regime accessible to spICP-MS.

Log α values for the PVP and PMMA, 3.45 and 2.17 respectively, suggest that there are roughly 10 times the number of PVP particles in solution compared to the PMMA. This is supported by the observation that the spICP-MS data for both the 10^2x and 10^3x dilutions of the PMMA have the minimum threshold of 1 count (threshold size: 0.22um), suggesting that there is no particle-based background present. In contrast, the dilutions PVP suspension has threshold sizes ranging from 0.54-0.1um that decrease with the level of dilution, suggesting the presence of a particle-based threshold. The presence of this particle-based background supports the observed differences in α that indicate the PVP suspension has a higher number of particles in solution than the PMMA. Thus the "artifact-free" PNC may be approached at the higher dilutions, but low counting statistics make the results less certain. Moreover, our results suggest that β and α values reflect real, physical differences between these two NP samples and may be used to compare their PSDs and PNCs.

Overall, we have shown that for these metal-tagged NPs in a series of serial dilutions, regions of usable, non-coincident ("artifact-free") data from each concentration-dependent PSD can be identified, combined, and modeled to create a global fit of the overall PSD. In this manner, a polydisperse sample can be analyzed, preserving information about the number distribution at larger sizes while simultaneously using higher dilutions to reduce threshold and accurately measure the lower end of the total size distribution. Functionally, this extends the size range of spICP-MS analysis roughly 10-fold compared to that measured in a single dilution. Furthermore, the method produces both β, describing the shape of the PSD across the entire measured size range, and α representing the total particle concentration distributed across all sizes.

Monitoring Changes in PSD/PNC as a Function of Discharge for Al-bearing Stream Particles During a Storm Event

Having demonstrated the utility of serial dilutions to determine "artifact-free" PSDs for metal-tagged NPs, we show how this improved methodology can change our interpretation of data acquired on the resident particle populations in stream water during a hydrological event. The power law observed in natural colloids(24) and our results for the metal-tagged NPs support our view that unless a careful dilution study is made, background size cut-offs at any single dilution are likely impacted by the coincidence created by large numbers of small particles present in natural waters. As a result of this high concentration of small particles, coincidence effects will distort the PSD and PNC determined by spICP-MS, which will go undetected in a more conventional, single dilution spICP-MS approach. To demonstrate the existence of this issue, we illustrate how conclusions regarding environmental processes in our stream study can be very different when using the comprehensive multiple dilution and single-dilution spICP-MS(42–46) approaches. In our example, Al-containing NMs and colloids were sampled from Cherry Creek, Denver CO USA (5/19/22 – 5/23/22) where storm discharge (Q, cfs) increased by as much as 10-fold (SI Fig S1). Figure 5 shows spICP-MS PSD analysis of the different samples collected across this major storm event and measured at a single dilution (10^2x). Particle size

detection thresholds are displayed in a table below the figure. Two of the samples, 5/20 and 5/21, show particularly high thresholds compared to the other samples, suggesting the presence of a coincident particle background at this dilution (Fig 1). As a point of comparison, we also measured PSDs at different dilutions to create overlapping size-distributions (example given in Figure 6), thereby generating "artifact-free" PSDs and power law models that avoid distortion by particle coincidence.

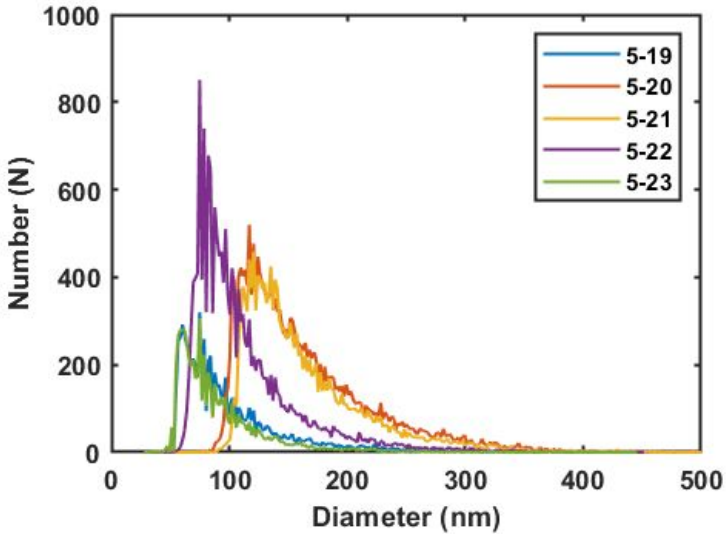

Sampling Date	**5/19**	**5/20**	**5/21**	**5/22**	**5/23**
Threshold (nm)	17	29	34	20	21

Figure 5. spICP-MS results for a single 10^2x dilution (all dates) of Al-bearing colloids collected from Cherry Creek, CO USA across a major storm event. The table shows the calculated threshold particle size for each sample. Particle diameters reflect a conversion of the detected Al mass to the diameter of an equivalently sized K-Feldspar particle.

Analysis of Storm-Influenced Stream Particle Populations

(i) Using Serial Dilutions. Log-transformed PSDs from a dilution series of each of the five dates (Figure S6) were modeled to determine β and log α values for each sample collected during the event. Data from two dilutions (5/19, 5/22 and 5/23 samples), or three dilutions (5/20 and 5/21 samples) were combined to generate a power law model for each sample (SI Table S4, SI Figures S6, S7). An example of this analysis is shown in Figure 6. Only two dilutions were used for the 5/19, 5/22 and 5/23 samples as low PNC made it impossible to dilute the sample more than 3 orders of magnitude and still count sufficient particle numbers. Figure S6 demonstrates that regions of "artifact-free" PSD data were identified for each of the samples and by regression analysis this data, we show that a power law relationship does indeed describe the PNC for all sampling dates. Log α values (Fig 7a) indicate that PNC increases with storm discharge (Q, cfs), peaks at 11 commensurate with maximum Q (119 cfs) and remained elevated post-storm (5/22, 5/23) compared to the pre-storm (5/19) PNC value. β values (Fig 7b) become more negative with increasing discharge, reaching a minimum, -3.97, at maximum Q, and remain suppressed post-storm compared to pre-storm. This decrease in β indicates that the elevated discharge during the storm is preferentially mobilizing smaller-sized (fine) particulates as compared to those mobilized by the constant discharge pre-storm.

Taken together, these power law relationships and their associated log α and β values measured herein support a simple model for how the characteristics of the particle population are driven by Q. On the ascending limb of the hydrograph (5/19-5/21) a strong linear relationship is observed between log α and Q (Figure 7a). During this period β becomes more negative but the relationship is not as strongly linear (Figure 7b). On the descending limb (5/21-5/23) a generally opposite trend is observed but changes in α and β are not as linear with respect to Q (Figure 7 a,b). In other words, storm mobilized particulates are both greater in number and included a higher proportion of small particles compared to pre-storm, with some elevated amounts of material being transported by the waterway post-storm.

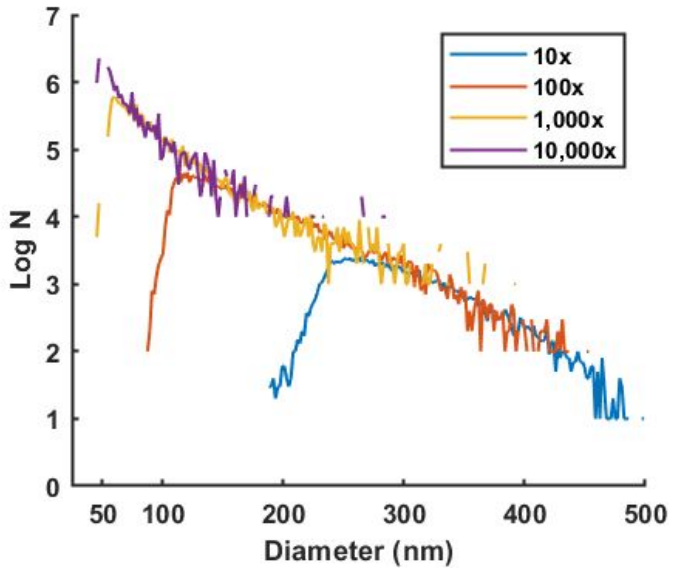

Figure 6. Example log-log plot (5/21 data) used for power law analysis of Cherry Creek storm samples. Particle numbers are corrected for the dilution factor.

For these environmental colloids, β and log α values were similar to those calculated for particles with diameters in the micron range (2-13um) during similar short-term, high-discharge events (52) suggesting that the micro- to nanoscale trends in this study may extend into the micron range. Power law modeling has been undertaken in the past for the purposes of modeling aerosol, freshwater and marine colloids [58, 24, 51) producing a wide range of alpha and beta constants depending on the system in question. Our results fit within this framework.

(ii) Traditional Single Dilution spICP-MS Analysis. A traditional spICP-MS analysis typically focuses on reporting PNC and mean particle diameter (e.g. Figure 6), and is often obtained from a single dilution. A potential problem with this type of analysis may occur when particle concentration varies among different samples (e.g. acquired in our case at different points along the storm's progression) to the point that unequal thresholds are present. This would result in PNC and PSD that are inconsistent within the sample set. To illustrate that this potential issue is operative for our river study, we analyzed data from only the 10^2x dilution (Fig 5a) to determine PNC (Fig 7c) and mean particle diameter (Fig 7d). Reported mean particle diameter and PNC increased with Q, peaking at 164nm and 9.5 x10^5 part/mL, respectively, at the second highest Q (90cfs). PNC (Fig 7c) values decreased at maximum discharge, remaining near constant post-storm (5/22), before ending at a value lower than measured pre-storm. This pattern thus shows only a weak dependence of PNC on Q, which is contrary to reasonable expectations given the introduction of particles from surface runoff and sediment resuspension during the storm. Mean particle size follows a similar trend, increasing commensurate with discharge, but with little difference during the storm (5/20 and 5/21), before falling off as discharge returns to pre-storm levels. As discussed previously, the elevated thresholds of the 10^2x dilutions of the 5/20 and 5/21 likely

arise from coincident small particles in these samples and cause a distortion in the measured PSDs and PNCs in the 10^2x dilutions.

Comparison of PNC vs Log α. Log α values obtained from the power law analysis using serial dilutions reflect particle number and therefore can be meaningfully compared to the PNC data acquired using a single dilution. Comparing trends in the log α values and the PNC measured from a single dilution, log α peaks with peak Q (117cfs), while in contrast, PNC peaks during a day earlier at the second highest Q (90cfs). The behavior in PNC obtained from the single dilution is contrary to the expectations of particle introduction from surface runoff and sediment resuspension accompanying the storm. Resuspension of bed sediments and influxes of material from neighboring terrain should be maximal at maximum

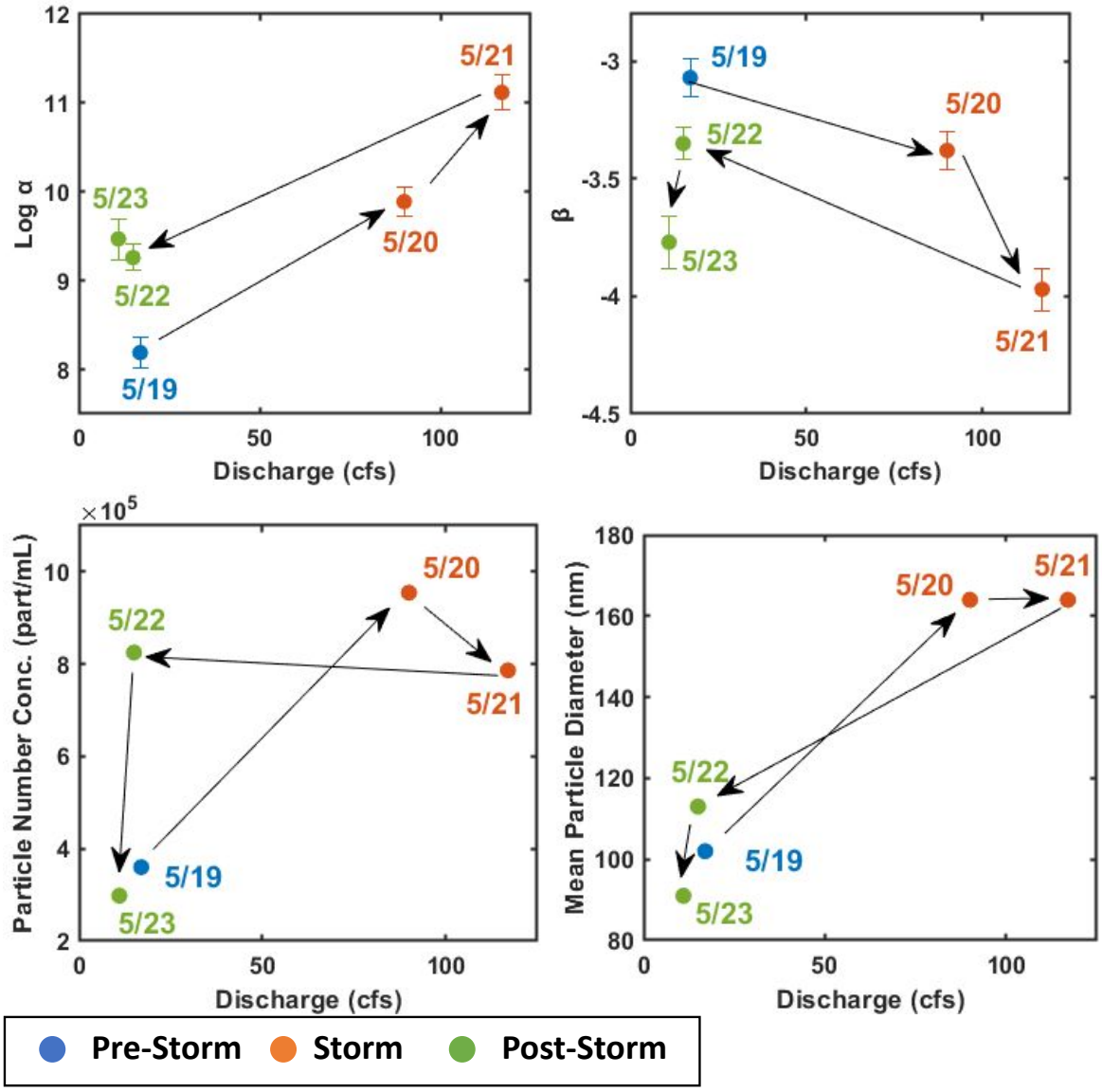

Figure 7. (a)Log α values and (b) β values were derived from the power law modeling of a dilution series for each date (data in SI). (c) PNC acquired from a single dilution (10^2x) across all samples (d) mean particle size acquired from a single dilution (10^2x) across all samples. Arrows show the temporal relationships among the samples and sampling dates of each data point labeled in panels (a-d).

discharge. Additionally, PNC returns to a final post-storm value lower than pre-storm value which is also unlikely to reflect the actual situation, because PNC numbers would be expected to return to close to pre-storm levels. These differences in PNC behavior with respect to Q are likely artifactual and can be attributed to under-counting of the smaller particles in the 10^2x dilution of the 5/21 and 5/23 samples as a result of particle coincidence.

The issue with the single dilution measurements is also evidenced by the observation that the PNC obtained by a single dilution only varies within about an order of magnitude across all dates even though variation in log α suggests particle number concentration varies by > 4 orders of magnitude (Figure S7). This insensitivity to PNC for the single dilution analysis can be rationalized by recognizing that as the storm progressed, the fine particles that are being introduced lead to increased particle coincidence. As a result, the true difference in PNC across the samples are obscured in the 10^2x dilutions due to varying levels of particle coincidence. This makes it clear that the power law modeling, which necessitates the identification and exclusion of data distorted by particle coincidence using serial dilutions, allows for a more accurate accounting of PNC variation in these measured samples.

Comparison of Mean Particle Size to β. Mean particle diameter values obtained from single dilution data and β values (which reflects particle size distribution) obtained from serial dilutions show opposite trends. Thus, β values obtained from serial dilutions decrease with increasing discharge (Fig 5b), revealing that the proportion of small to large particles is increasing over the course of the event and persists post-storm. In contrast, the mean particle diameter, measured from the single 10^2x dilutions of each sample (Fig 5d), increased with discharge before plateauing and ending at smaller value than pre-storm. Again, the difference in trends between the two analytical approaches can be attributed to the effect of coincidence on the particle-based backgrounds in the 5/20 and 5/21 samples. This unwanted effect causes an erroneous undercounting of the smaller-sized particles, whose omission skews the mean particle diameter to artificially higher values in the single dilution analysis. Using β values from serial dilution measurements which are free of distortion due to particle coincidence provides a more accurate assessment of the PSD as well as changes to the proportion of small to large particles between samples. Moreover, the availability of accurate particle size and number from serial dilution experiments also improves estimates of total colloidal mass and surface area. For example, for the 5/23 sample, using a single dilution for spICP-MS analysis results in an underestimation of total mass in particles by 22% and total particle surface area (assuming a spherical shape) by 23% compared to the power law model for the same sample, acquired using the serial dilution method developed in this manuscript.

Conclusions

Nanoparticles and colloids are important components of natural and human-impacted environments, with size playing an influential role in their environmental reactivity, fate, and transport. Key particulate classes include natural (e.g. clays, metal oxides), incidental (soot, tire wear, nanoplastic), and engineered (gold, quantum dots). The processes that generate and transport nanoparticles and colloids also result in broad size distributions. Accurate measurement of PSD that span orders of magnitude (nm to micron) is critical to our understanding of their behavior. Our proposed analysis methodology is advantageous in that particle numbers and PSDs are corrected for the deleterious effects of particle coincidence, especially at the smallest region of the PSD, by combining data from multiple dilutions.

As an illustrative example of where improved information on PSD and PNC matters, consider particle toxicity which depends on the properties of the nanomaterial in question, but also requires an accurate particle number for calculating dosage, and subsequently evaluating a nanomaterial in a toxicity assay. Total particle mass, measured through filtration or other bulk means, is an incomplete measure of PNC as a given mass could contain a wide range of particle concentrations depending on particle size. Without an accurate measurement of particle number and thereby particle dose, the relative toxicity of nanomaterial cannot be compared to another toxicant. For example, consider the characterization of aerosolized ultrafine (PM0.1) particles, which are of concern to fields as diverse as human health(16) and climate science(17). These particles exist transiently at high, local concentrations making particle coincidence likely in their measurement, rendering particle number difficult to accurately to assess.

Techniques such as SPOS(56) or time-of-flight single particle mass spectrometers(57) struggle with coincidence in a similar manner to spICP-MS leading to the exclusion of data taken at high particle concentrations and use of high dilutions in routine analysis. As we discussed previously, these high dilution factors lead to a degradation of particle numbers measured for lower abundance, larger particles. The methodology proposed herein could be used similarly for data obtained using other single particle methods in order to identify coincidence-distorted data in samples with high total particle numbers. Furthermore, as demonstrated by the storm colloids in this manuscript, employing our methodology can lead to more accurate determination of particle number over a wider size range for high concentration samples.

Lastly, power law modeling has been undertaken in the past for the purposes of modeling aerosol, freshwater and marine colloids(24,51,58). Single particle ICP-MS can often detect and size particles smaller in size than many other single particle techniques. By combining this sensitive technique with power law modeling, we can measure size distributions that are independent of the technique itself and can be compared to power law models derived from alternate techniques. For example, the influence of discharge on the β and log α values determined for the storm-colloids in this study showed reasonable agreement with those calculated for larger 2-13um particles during similar short-term, high-discharge events measured with by a light-blocking laser particle sizer(52). Combining the data of a particle sizer such as SPOS to measure larger particles with that of spICP-MS(47) can extend the characterizable size range and enhance our understanding of the entire colloidal population.

Acknowledgments

This work was supported by the National Science Foundation (Grant No. 2003481). Additionally, the SEM and µXRF measurements were performed in the Minerals and Materials Characterization Facility at Colorado School of Mines with the assistance of Dr. Katharina Pfaff and Kelsey Livingston.

References.

1. Roduner E. Size matters: why nanomaterials are different. Chem Soc Rev. 2006;35(7):583.

2. Montanarella F, Kovalenko MV. Three Millennia of Nanocrystals. ACS Nano. 2022 Apr 26;16(4):5085–102.

3. Lee JH, Huh YM, Jun Y wook, Seo J wook, Jang J tak, Song HT, et al. Artificially engineered magnetic nanoparticles for ultra-sensitive molecular imaging. Nat Med. 2007 Jan;13(1):95–9.

4. Almeida MS de, Susnik E, Drasler B, Taladriz-Blanco P, Petri-Fink A, Rothen-Rutishauser B. Understanding nanoparticle endocytosis to improve targeting strategies in nanomedicine. Chemical Society Reviews. 2021;50(9):5397–434.

5. Servin A, Elmer W, Mukherjee A, De la Torre-Roche R, Hamdi H, White JC, et al. A review of the use of engineered nanomaterials to suppress plant disease and enhance crop yield. J Nanopart Res. 2015 Feb;17(2):92.

6. Hochella MF, Mogk DW, Ranville J, Allen IC, Luther GW, Marr LC, et al. Natural, incidental, and engineered nanomaterials and their impacts on the Earth system. Science. 2019 Mar 29;363(6434):eaau8299.

7. Gu B, Schmitt J, Chen Z, Liang L, McCarthy JF. Adsorption and desorption of different organic matter fractions on iron oxide. Geochimica et Cosmochimica Acta. 1995 Jan;59(2):219–29.

8. Liu G, Dave PH, Kwong RWM, Wu M, Zhong H. Influence of Microplastics on the Mobility, Bioavailability, and Toxicity of Heavy Metals: A Review. Bull Environ Contam Toxicol. 2021 Oct;107(4):710–21.

9. Hassellöv M, Kammer F von der. Iron Oxides as Geochemical Nanovectors for Metal Transport in Soil-River Systems. Elements. 2008 Dec 1;4(6):401–6.

10. Maurer-Jones MA, Gunsolus IL, Murphy CJ, Haynes CL. Toxicity of Engineered Nanoparticles in the Environment [Internet]. ACS Publications. American Chemical Society; 2013 [cited 2023 Jan 18]. Available from: https://pubs.acs.org/doi/pdf/10.1021/ac303636s

11. Rizzolo JA, Barbosa CGG, Borillo GC, Godoi AFL, Souza RAF, Andreoli RV, et al. Soluble iron nutrients in Saharan dust over the central Amazon rainforest. Atmos Chem Phys. 2017 Feb 22;17(4):2673–87.

12. Gigault J, El Hadri H, Nguyen B, Grassl B, Rowenczyk L, Tufenkji N, et al. Nanoplastics are neither microplastics nor engineered nanoparticles. Nat Nanotechnol. 2021 May;16(5):501–7.

13. Ma H, Pu S, Liu S, Bai Y, Mandal S, Xing B. Microplastics in aquatic environments: Toxicity to trigger ecological consequences. Environmental Pollution. 2020 Jun 1;261:114089.

14. Riediker M, Zink D, Kreyling W, Oberdörster G, Elder A, Graham U, et al. Particle toxicology and health - where are we? Part Fibre Toxicol. 2019 Dec;16(1):19.

15. Lead JR, Batley GE, Alvarez PJJ, Judy JD, Schirmer K. Nanomaterials in the environment: Behavior, fate, bioavailability, and effects—An updated review. Environmental Toxicology and Chemistry. 2018;35.

16. Schraufnagel DE. The health effects of ultrafine particles. Exp Mol Med. 2020 Mar;52(3):311–7.

17. Kwon HS, Ryu MH, Carlsten C. Ultrafine particles: unique physicochemical properties relevant to health and disease. Exp Mol Med. 2020 Mar;52(3):318–28.

18. US EPA O. Drinking Water Regulations [Internet]. 2015 [cited 2023 Apr 22]. Available from: https://www.epa.gov/dwreginfo/drinking-water-regulations

19. Berne BJ, Pecora R. Dynamic Light Scattering: With Applications to Chemistry, Biology, and Physics. Courier Corporation; 2000. 388 p.

20. L. Planken K, Cölfen H. Analytical ultracentrifugation of colloids. Nanoscale. 2010;2(10):1849–69.

21. Schimpf ME, Caldwell K, Giddings JC. Field-Flow Fractionation Handbook. John Wiley & Sons; 2000. 618 p.

22. Kim A, Ng WB, Bernt W, Cho NJ. Validation of Size Estimation of Nanoparticle Tracking Analysis on Polydisperse Macromolecule Assembly. Sci Rep. 2019 Feb 25;9(1):2639.

23. White DJ. PSD measurement using the single particle optical sizing (SPOS) method. Géotechnique. 2003 Apr;53(3):317–26.

24. Buffle J, Leppard GG. Characterization of Aquatic Colloids and Macromolecules. 1. Structure and Behavior of Colloidal Material. Environ Sci Technol. 1995 Sep 1;29(9):2169–75.

25. Junge C. THE SIZE DISTRIBUTION AND AGING OF NATURAL AEROSOLS AS DETERMINED FROM ELECTRICAL AND OPTICAL DATA ON THE ATMOSPHERE. Journal of the Atmospheric Sciences. 1955 Feb 1;12(1):13–25.

26. Bittelli M, Campbell GS, Flury M. Characterization of Particle-Size Distribution in Soils with a Fragmentation Model. Soil Sci Soc Am J. 1999 Jul;63(4):782–8.

27. Maring H. Mineral dust aerosol size distribution change during atmospheric transport. J Geophys Res. 2003;108(D19):8592.

28. Pace HE, Rogers NJ, Jarolimek C, Coleman VA, Higgins CP, Ranville JF. Determining Transport Efficiency for the Purpose of Counting and Sizing Nanoparticles via Single Particle Inductively Coupled Plasma Mass Spectrometry. Anal Chem. 2011 Dec 15;83(24):9361–9.

29. Montaño MD, Olesik JW, Barber AG, Challis K, Ranville JF. Single Particle ICP-MS: Advances toward routine analysis of nanomaterials. Anal Bioanal Chem. 2016 Jul 1;408(19):5053–74.

30. Mozhayeva D, Engelhard C. A critical review of single particle inductively coupled plasma mass spectrometry – A step towards an ideal method for nanomaterial characterization. Journal of Analytical Atomic Spectrometry. 2020;35(9):1740–83.

31. Bolea E, Jimenez MS, Perez-Arantegui J, Vidal JC, Bakir M, Ben-Jeddou K, et al. Analytical applications of single particle inductively coupled plasma mass spectrometry: a comprehensive and critical review. Anal Methods. 2021 Jul 2;13(25):2742–95.

32. Tuoriniemi J, Cornelis G, Hassellöv M. Size Discrimination and Detection Capabilities of Single-Particle ICPMS for Environmental Analysis of Silver Nanoparticles. Anal Chem. 2012 May 1;84(9):3965–72.

33. Liu J, Murphy KE, MacCuspie RI, Winchester MR. Capabilities of Single Particle Inductively Coupled Plasma Mass Spectrometry for the Size Measurement of Nanoparticles: A Case Study on Gold Nanoparticles. Anal Chem. 2014 Apr 1;86(7):3405–14.

34. Abad-Álvaro I, Peña-Vázquez E, Bolea E, Bermejo-Barrera P, Castillo JR, Laborda F. Evaluation of number concentration quantification by single-particle inductively coupled plasma mass spectrometry: microsecond vs. millisecond dwell times. Anal Bioanal Chem. 2016 Jul;408(19):5089–97.

35. Hendriks L, Gundlach-Graham A, Günther D. Performance of sp-ICP-TOFMS with signal distributions fitted to a compound Poisson model. Journal of Analytical Atomic Spectrometry. 2019;34(9):1900–9.

36. Lee S, Bi X, Reed RB, Ranville JF, Herckes P, Westerhoff P. Nanoparticle Size Detection Limits by Single Particle ICP-MS for 40 Elements. Environ Sci Technol. 2014 Sep 2;48(17):10291–300.

37. Fréchette-Viens L, Hadioui M, Wilkinson KJ. Quantification of ZnO nanoparticles and other Zn containing colloids in natural waters using a high sensitivity single particle ICP-MS. Talanta. 2019 Aug 1;200:156–62.

38. Montaño MD, Majestic BJ, Jämting ÅK, Westerhoff P, Ranville JF. Methods for the Detection and Characterization of Silica Colloids by Microsecond spICP-MS. Anal Chem. 2016 May 3;88(9):4733–41.

39. Laborda F, Trujillo C, Lobinski R. Analysis of microplastics in consumer products by single particle-inductively coupled plasma mass spectrometry using the carbon-13 isotope. Talanta. 2021 Jan;221:121486.

40. Hineman A, Stephan C. Effect of dwell time on single particle inductively coupled plasma mass spectrometry data acquisition quality. J Anal At Spectrom. 2014 Jun 13;29(7):1252–7.

41. Donahue ND, Francek ER, Kiyotake E, Thomas EE, Yang W, Wang L, et al. Assessing nanoparticle colloidal stability with single-particle inductively coupled plasma mass spectrometry (SP-ICP-MS). Anal Bioanal Chem. 2020 Sep;412(22):5205–16.

42. Peters RJB, van Bemmel G, Milani NBL, den Hertog GCT, Undas AK, van der Lee M, et al. Detection of nanoparticles in Dutch surface waters. Science of The Total Environment. 2018 Apr 15;621:210–8.

43. Bevers S, Montaño M, Rybicki L, Hofmann T, Kammer F von der, Ranville J. Quantification and Characterization of Nanoparticulate Zinc in an Urban Watershed. Frontiers in Environmental Science: Biogeochemical Dynamics [Internet]. 2020 Jun 18;8. Available from: https://cedar.wwu.edu/esci_facpubs/61

44. Azimzada A, M. Farner J, Hadioui M, Liu-Kang C, Jreije I, Tufenkji N, et al. Release of TiO 2 nanoparticles from painted surfaces in cold climates: characterization using a high sensitivity single-particle ICP-MS. Environmental Science: Nano. 2020;7(1):139–48.

45. Alshehri T, Wang J, Singerling SA, Gigault J, Webster JP, Matiasek SJ, et al. Wildland-urban interface fire ashes as a major source of incidental nanomaterials. Journal of Hazardous Materials. 2023 Feb 5;443:130311.

46. Mansor M, Drabesch S, Bayer T, Van Le A, Chauhan A, Schmidtmann J, et al. Application of Single-Particle ICP-MS to Determine the Mass Distribution and Number Concentrations of Environmental Nanoparticles and Colloids. Environ Sci Technol Lett. 2021 Jul 13;8(7):589–95.

47. Goodman AJ, Gundlach-Graham A, Bevers SG, Ranville JF. Characterization of nano-scale mineral dust aerosols in snow by single particle inductively coupled plasma mass spectrometry. Environ Sci: Nano. 2022 Aug 11;9(8):2638–52.

48. Laborda F, Jiménez-Lamana J, Bolea E, Castillo JR. Critical considerations for the determination of nanoparticle number concentrations, size and number size distributions by single particle ICP-MS. J Anal At Spectrom. 2013;28(8):1220.

49. Domingos RF, Rafiei Z, Monteiro CE, Khan MAK, Wilkinson KJ. Agglomeration and dissolution of zinc oxide nanoparticles: role of pH, ionic strength and fulvic acid. Environ Chem. 2013 Aug 2;10(4):306–12.

50. Huynh KA, Siska E, Heithmar E, Tadjiki S, Pergantis SA. Detection and Quantification of Silver Nanoparticles at Environmentally Relevant Concentrations Using Asymmetric Flow Field–Flow Fractionation Online with Single Particle Inductively Coupled Plasma Mass Spectrometry. Anal Chem. 2016 May 3;88(9):4909–16.

51. Xi H, Larouche P, Tang S, Michel C. Characterization and variability of particle size distributions in Hudson Bay, Canada. J Geophys Res Oceans. 2014 Jun;119(6):3392–406.

52. Cristina CM, Sansalone JJ. "First Flush," Power Law and Particle Separation Diagrams for Urban Storm-Water Suspended Particulates. J Environ Eng. 2003 Apr;129(4):298–307.

53. Merrifield RC, Stephan C, Lead JR. Quantification of Au Nanoparticle Biouptake and Distribution to Freshwater Algae Using Single Cell – ICP-MS. Environ Sci Technol. 2018;7.

54. Tewari A, Almuhtaram H, McKie MJ, Andrews RC. Microplastics for Use in Environmental Research. J Polym Environ [Internet]. 2022 Jul 7 [cited 2022 Jul 20]; Available from: https://link.springer.com/10.1007/s10924-022-02519-w

55. Green JL, Petty CA, Grulke EA. Impact grinding of thermoplastics: A size distribution function model. Polym Eng Sci. 1997 May;37(5):888–95.

56. Raasch J, Umhauer H. Errors in the Determination of Particle Size Distributions Caused by coincidences in optical particle counters. Part Part Syst Charact. 1984;1(1–4):53–8.

57. Cross ES, Onasch TB, Canagaratna M, Jayne JT, Kimmel J, Worsnop DR, et al. Single particle characterization using a light scattering module coupled to a time-of-flight aerosol mass spectrometer. Atmos Chem Phys. 2009;

58. Kulkarni P, Baron PA, Willeke K. Aerosol Measurement: Principles, Techniques, and Applications. John Wiley & Sons; 2011. 904 p.